RETHINKING THE GENERALIZATION OF DRUG TARGET AFFINITY PREDICTION ALGORITHMS VIA SIMILARITY AWARE EVALUATION

Anonymous authors
Paper under double-blind review

ABSTRACT

Drug-target binding affinity prediction is a fundamental task for drug discovery. It has been extensively explored in literature and promising results are reported. However, in this paper we demonstrate that the results may be misleading and cannot be well generalized to real practice. The core observation is that the canonical randomized split of testset in conventional evaluation leaves the testset dominated by samples with high similarity to trainset. Performance of models is severely degraded on samples with lower similarity to trainset but the drawback is highly overlooked in current evaluation. As a result, the performance can hardly be trusted when the model meets low-similarity samples in real practice. To address this problem, we propose a framework of similarity aware evaluation in which a novel split methodology is proposed to adapt to any desired distribution. This is achieved by a formulation of optimization problems which are approximately and efficiently solved by gradient descent. We perform extensive experiments across five representative methods in four datasets for two typical target evaluation and compare with various counterpart methods. Results demonstrate that the proposed split methodology can significantly better fit desired distributions and guide the development of models.

1 INTRODUCTION

Drug-target binding affinity (DTA) prediction is a fundamental and crucial task for drug discovery. It evaluates effectiveness of drug candidates, or samples, and sees its application in large-scale virtual screening where majority of ineffective candidates are filtered out to save experimental cost and time (Chatterjee et al., 2023). DTA is quantitatively measured by inhibition constant Ki, half maximal inhibitory concentration IC50, etc., which are all real-valued (Monteiro et al., 2022). The prediction performance is commonly evaluated by mean absolute error (MAE) and coefficient of determination (R^2).

The task of DTA prediction has been extensively studied for decades (Chen et al., 2018; Askr et al., 2023). Related works can be categorized as structure-based, sequence-based and similarity-based (Wu et al., 2018; Chuang et al., 2020). Structure-based methods rely on 3D structures of samples, target proteins or their complexes. Although theoretically accessible to most comprehensive information following the dogma “structure determines function”, structure-based methods are limited by available 3D structures, especially experimentally verified structures, and also hindered in practice by poor time efficiency. On contrast, sequence-based and similarity-based methods are fast and do not set 3D structures as prerequisite (Xu et al., 2017; Zhang et al., 2022). Instead they take as input residual sequences, Simplified Molecular-Input Line-Entry System (SMILES) sequences, fingerprint sequences, atom-bond graphs or the derived pairwise similarities, which are easier to acquire with lower cost. Moreover, these sequences and similarities are readily processed by diversified sophisticated backbones including convolutional neural networks (CNNs) (Öztürk et al., 2018; Li et al., 2019; Hu et al., 2023), recurrent neural networks (RNNs) (Karimi et al., 2019; Yuan et al., 2022), graph neural networks (GNNs) (Nguyen et al., 2021; Yang et al., 2022; Tang et al., 2022; Wang et al., 2022) and transformers (Chithrananda et al., 2020; Zhao et al., 2022; Song et al., 2023; Jiang et al., 2023), and enjoy the benefits of the development of deep learning techniques. As a result, sequence-based and similarity-based methods are shown to reach new high performance and are drawing increasing attentions.

Although promising results are reported, we find, surprisingly, that these results may be misleading. Take the task of IC50 prediction for target EGFR as an example, as shown in Figure 1, we evaluate five state-of-the-art and representative methods and the best-performing one, SAM-DTA (Hu et al., 2023), achieves a MAE of 0.6012 and R^2 of 0.6505 for the *whole* testset. However, if we dive into the performance and divide the testset according to the similarity of the sample to the trainset, we find a clear performance degradation for low-similarity samples: the MAE deteriorates to 1.2970 for samples with similarity less than 1/3 and R^2 to -0.6385. The gap is huge. Nevertheless, poor performance on low-similarity samples does not really affect the *whole* performance since they only occupy a negligible proportion: only 16 samples with similarity less than 1/3 out of a total of 873 samples in testset (Figure 1). In other words, testset is dominated by high-similarity samples and performance for low-similarity samples are overwhelmed in current evaluations. We will show that the phenomenon exists across different similarity measures, performance metrics, datasets and methods, and therefore it is general. Consequently, the evaluation will be misleading to practitioners, especially when the trained model meets low-similarity samples when used in real practice.

We argue that the core of the problem lies in the canonical randomized split of testset. Randomized split follows the assumption of independent identically distribution (I.I.D.), which is the foundation of most statistical learning theories. However, in drug discovery samples are not necessarily independent to each other: in practice, mutually similar variants are more likely to be tested together in high-throughput experiments, while at the same time they have to avoid high similarity to approved drugs for intellectual property issues (Harren et al., 2024). Empirically, drugs developed at different times show significant distinction in their properties (Sheridan et al., 2022). As a result, practitioners would not always expect that samples they are going to test follow the same distribution as historical samples. This in turn raises a request to the model development that testset should satisfy a desired distribution. For example, one may need a testset that is uniform at different similarity bins; others may ask the testset samples to be all limited within predefined similarity bounds, and so on (Li & Yang, 2017; Simm et al., 2021; Luo et al., 2024; Tricarico et al., 2024).

We formulate the problem of testset split with a desired distribution as a combination optimization problem. The problem is infeasible to solve for optimum due to efficiency issues. In this work, we address this challenge by relaxing it to a continuous optimization problem where samples are allowed to coexist in trainset and testset with a “probability” or weight. Further, the objective function contains non-differentiable operations including taking the maximum and counting in similarity bins, and are approximated in this work by differentiable counterparts. We will show that the degree of approximation is adjustable by introduced hyper-parameters. Next, the resulting optimization problem has no closed-form solution, and hence we have resorted to Lagrangian multipliers with numerical method implemented by PyTorch and Cooper (Gallego-Posada & Ramirez, 2022). Finally, we analyze the continuously-valued solution and find the non-negligible approximation error induced by the relaxation. To this end, we introduce a regularization term that penalizes samples whose weight is far from bipartition. We refer to our strategy as **S**imilarity **A**ware **E**valuation, abbreviated as SAE. By doing all this, we have managed to achieve testset split with various desired distributions.

Extensive experiments are performed to substantiate the effectiveness of our split strategy. To begin with, our split strategy can achieve a uniformly distributed testset across various similarity bins (Figure 1). Subsequently, we evaluate the performance of five DTA prediction methods on this testset. The results underscore a distinct relationship between the performance and the corresponding similarity levels, suggesting a more comprehensive assessment of balanced split across varied methods in comparison to the strategy of randomized split. Moreover, in scenarios where the samples practitioners intend to test deviate from the distribution of existing samples, our split strategy can effectively split the trainset and internal testset based on the similarity distribution of the testset (Figure 4). Here we conduct hyper-parameter searches on the internal testset set across five DTA prediction methods to assess the efficacy of our split strategy. Compared to previous split strategies, our split strategy facilitates the selection of optimal hyper-parameters, enhancing performance on the external testset (Figure 5). In other scenarios where practitioners specify predefined similarity constraints for the testset samples, such as a maximum similarity limit of 0.4 or 0.6, or even a range bounded by a minimum and maximum similarity of 0.4 and 0.6, our split strategy ensures the majority of samples in the testset adhering to these requirements (Figure 6).

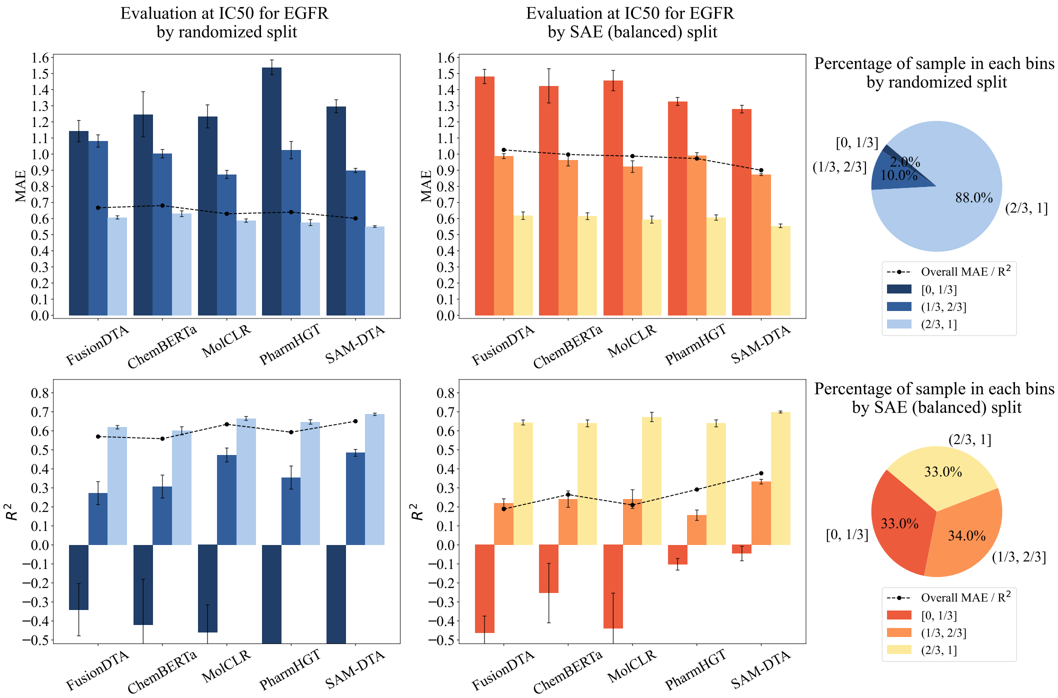

Figure 1: Comparison of randomized split and SAE (balanced) split at IC50 for EGFR. The randomized split led to 88% of test samples yielding a high similarity ($> 2/3$) to the trainset. In contrast, our SAE (balanced) split strategy ensures a more balanced distribution of similarities. The evaluation of five DTA prediction methods demonstrates that the performance aligns with the similarity levels. In the randomized split, the overall performance closely resembles that of high-similarity samples, thus failing to evaluate the performance when encountering low-similarity samples.

2 PROBLEM OF RANDOMIZED SPLIT

In this section we will show that the imbalanced distribution of samples and the consequent overwhelming of low-similarity samples is general for randomized split of testset across different similarity measures, performance metrics, datasets and methods. We will firstly give the details of the example in Figure 1, and then explore possible variants.

In the example demonstrated by Figure 1, we take the IC50 dataset of target EGFR with a total of 4,361 samples, which is one of the largest dataset we are able to find. The dataset has originated from the BindingDB database, and IC50 has been converted to its negative logarithm form, $pIC50 = -\log_{10} IC50\ (Molar)$ following the convention. Then, we randomly split the dataset into trainset and testset with a ratio of 8:2. Subsequently, we train and validate the DTA prediction models on the trainset and evaluate their performance on the testset. It should be noted that we follow the original hyper-parameter tuning procedure as outlined in the source code of each DTA prediction method.

To perform the fine-grained evaluation with respect to the similarity, we firstly define the pairwise similarity for sample x_1 and x_2,

$$PairwiseSimlarity(x_1, x_2) = SimilarityMeasure\left(Feature(x_1), Feature(x_2)\right) \tag{1}$$

and then derive the similarity to the union of the trainset by aggregation, for sample $x \in testset$.

$$SimlarityToTrainset(x) = \underset{t \in trainset}{Aggregation}\ PairwiseSimlarity(x, t) \tag{2}$$

where in the example of Figure 1, we set $Feature$ as the Morgan fingerprint and $SimilarityMeasure$ as the Tanimoto coefficient, which are both commonly used to measure the similarity of samples, and we set $Aggregation$ as the maximum function (Bajusz et al., 2015; Ying et al., 2021).

Table 1: Variations of $\mathit{SimilarityToTrainset}$ related to feature extraction, similarity measure, aggregation functions, and performance metrics. We choose PharmHGT and SAM-DTA as the example methods for the detailed showcase.

Randomized Split (MAE)						
Bin	Feature: RDKit fingerprint			Feature: Avalon fingerprint		
	Count (Ratio)	PharmHGT	SAM-DTA	Count (Ratio)	PharmHGT	SAM-DTA
[0, 1/3]	8 (0.0092)	1.7551	1.6787	0 (0.0000)	-	-
(1/3, 2/3]	34 (0.0389)	1.3214	1.0040	28 (0.0321)	1.4646	1.3319
(2/3, 1]	831 (0.9519)	0.6015	0.5743	845 (0.9679)	0.6128	0.5770
overall	873 (1.0000)	0.6401	0.6012	873 (1.0000)	0.6401	0.6012
	SimilarityMeasure: Sokal similarity			SimilarityMeasure: Dice coefficient		
[0, 1/3]	33 (0.0378)	1.5051	1.2444	0 (0.0000)	-	-
(1/3, 2/3]	398 (0.4559)	0.7066	0.6619	33 (0.0378)	1.5051	1.2444
(2/3, 1]	442 (0.5063)	0.5157	0.4985	840 (0.9622)	0.6061	0.5759
overall	873 (1.0000)	0.6401	0.6012	873 (1.0000)	0.6401	0.6012
	Aggregation: Top-3			Aggregation: Top-5		
[0, 1/3]	17 (0.0195)	1.5188	1.3149	24 (0.0275)	1.5627	1.3469
(1/3, 2/3]	171 (0.1959)	0.8890	0.7748	240 (0.2749)	0.8014	0.7228
(2/3, 1]	685 (0.7847)	0.5562	0.5401	609 (0.6976)	0.5402	0.5239
overall	873 (1.0000)	0.6401	0.6012	873 (1.0000)	0.6401	0.6012
Randomized Split (R^2)						
Bin	Feature: RDKit fingerprint			Feature: Avalon fingerprint		
	Count (Ratio)	PharmHGT	SAM-DTA	Count (Ratio)	PharmHGT	SAM-DTA
[0, 1/3]	8 (0.0092)	0.1555	0.2579	0 (0.0000)	-	-
(1/3, 2/3]	34 (0.0389)	-0.0371	0.3529	28 (0.0321)	0.1028	0.2921
(2/3, 1]	831 (0.9519)	0.6327	0.6706	845 (0.9679)	0.6169	0.6672
overall	873 (1.0000)	0.5928	0.6505	873 (1.0000)	0.5928	0.6505
	SimilarityMeasure: Sokal similarity			SimilarityMeasure: Dice coefficient		
[0, 1/3]	33 (0.0378)	-0.1562	0.1866	0 (0.0000)	-	-
(1/3, 2/3]	398 (0.4559)	0.5412	0.6057	33 (0.0378)	-0.1562	0.1866
(2/3, 1]	442 (0.5063)	0.6942	0.7156	840 (0.9622)	0.6290	0.6711
overall	873 (1.0000)	0.5928	0.6505	873 (1.0000)	0.5928	0.6505
	Aggregation: Top-3			Aggregation: Top-5		
[0, 1/3]	17 (0.0195)	-0.6280	-0.3148	24 (0.0275)	-0.2379	0.0891
(1/3, 2/3]	171 (0.1959)	0.4283	0.5743	240 (0.2749)	0.4756	0.5794
(2/3, 1]	685 (0.7847)	0.6483	0.6712	609 (0.6976)	0.6584	0.6804
overall	873 (1.0000)	0.5928	0.6505	873 (1.0000)	0.5928	0.6505

We next compare other variants for these functions. For the feature extractor $\mathit{Feature}$, we compare other widely used molecular descriptors including Avalon fingerprint and RDKit fingerprint (a.k.a. topological fingerprint); for the function $\mathit{SimilarityMeasure}$ we compare Sokal similarity and Dice coefficient, which are both symmetric for its parameters; and finally for the $\mathit{Aggregation}$ function, we compare the general top-k averaging where the maximum function can be seen as a special case of $k = 1$. Note that averaging or taking the median over the whole trainset is not suitable. This is because majority of samples in trainset have a low similarity to a specific sample, and averaging or taking the median over the whole trainset is not able to tell whether there exists any high-similarity ones. The results are shown in Table 1, here we choose two example methods for detailed showcase (PharmHGT (Jiang et al., 2023) and SAM-DTA (Hu et al., 2023)), while the results of other methods can be found in the appendix.

Table 2: Comparison of Randomized Split and SAE (balanced) Split at IC50 for BACE1, Ki for Carbonic anhydrase I and Carbonic anhydrase II. We choose PharmHGT and SAM-DTA as the example methods for the detailed showcase.

IC50 for Target BACE1 (MAE)						
Bin	Randomized Split			SAE (balanced) Split		
	Count (Ratio)	PharmHGT	SAM-DTA	Count (Ratio)	PharmHGT	SAM-DTA
[0 , 1/3]	10 (0.0108)	1.3743	1.1204	309 (0.3330)	1.1397	1.0309
(1/3, 2/3]	67 (0.0722)	0.6334	0.6928	311 (0.3351)	0.6410	0.6693
(2/3, 1]	851 (0.9170)	0.4611	0.4594	308 (0.3319)	0.4747	0.4808
overall	928 (1.0000)	0.4834	0.4834	928 (1.0000)	0.7518	0.7272
IC50 for Target BACE1 (R^2)						
[0 , 1/3]	10 (0.0108)	-0.0553	0.3702	309 (0.3330)	-0.2983	-0.1261
(1/3, 2/3]	67 (0.0722)	0.6789	0.6439	311 (0.3351)	0.5848	0.5637
(2/3, 1]	851 (0.9170)	0.7113	0.7150	308 (0.3319)	0.7797	0.7803
overall	928 (1.0000)	0.7190	0.7256	928 (1.0000)	0.5329	0.5665
Ki for Target Carbonic anhydrase I (MAE)						
Bin	Randomized Split			SAE (balanced) Split		
	Count (Ratio)	PharmHGT	SAM-DTA	Count (Ratio)	PharmHGT	SAM-DTA
[0 , 1/3]	7 (0.0079)	1.1467	0.8798	264 (0.2983)	0.8410	0.8729
(1/3, 2/3]	205 (0.2316)	0.5843	0.6605	311 (0.3514)	0.6706	0.6877
(2/3, 1]	673 (0.7605)	0.4986	0.4896	310 (0.3503)	0.6039	0.5740
overall	885 (1.0000)	0.5236	0.5323	885 (1.0000)	0.6981	0.7031
Ki for Target Carbonic anhydrase I (R^2)						
[0 , 1/3]	7 (0.0079)	-0.3232	0.1308	264 (0.2983)	-0.0389	-0.0282
(1/3, 2/3]	205 (0.2316)	0.5733	0.4820	311 (0.3514)	0.3642	0.3478
(2/3, 1]	673 (0.7605)	0.5037	0.5270	310 (0.3503)	0.3917	0.4262
overall	885 (1.0000)	0.5257	0.5174	885 (1.0000)	0.2994	0.3071
Ki for Target Carbonic anhydrase II (MAE)						
Bin	Randomized Split			SAE (balanced) Split		
	Count (Ratio)	PharmHGT	SAM-DTA	Count (Ratio)	PharmHGT	SAM-DTA
[0 , 1/3]	8 (0.0087)	0.5879	0.6645	244 (0.2667)	1.0450	1.0564
(1/3, 2/3]	201 (0.2197)	0.6807	0.7009	342 (0.3738)	0.7389	0.7572
(2/3, 1]	706 (0.7716)	0.5615	0.5426	329 (0.3596)	0.6172	0.5813
overall	915 (1.0000)	0.5879	0.5785	915 (1.0000)	0.7768	0.7738
Ki for Target Carbonic anhydrase II (R^2)						
[0 , 1/3]	8 (0.0087)	0.6739	0.4277	244 (0.2667)	-0.0885	0.0087
(1/3, 2/3]	201 (0.2197)	0.5803	0.5742	342 (0.3738)	0.4657	0.4690
(2/3, 1]	706 (0.7716)	0.5509	0.5932	329 (0.3596)	0.4760	0.5346
overall	915 (1.0000)	0.5684	0.5938	915 (1.0000)	0.3776	0.4192

For the prediction method, as shown in Figure 1, we select five state-of-the-art and representative DTA prediction methods. Molecular Contrastive Learning of Representations (MolCLR) sees samples as atom-bond graphs, and employs GCN and GIN to learn the molecular representations by contrastive pairs (Wang et al., 2022). Sequence-agnostic model for drug-target binding affinity prediction (SAM-DTA), on contrast, takes as input the Simplified Molecular-Input Line-Entry System (SMILES) of samples, and processes it using 1D-CNN with dilated parallel residual blocks (Hu et al., 2023). SMILES is also utilized in FusionDTA, but is processed by a unified LSTM model with linear attention mechanism (Yuan et al., 2022). Finally, we include two transformer-based methods. One is ChemBERTa which takes as input SMILES of samples and builds a model with

12 attention heads and 6 layers (Chithrananda et al., 2020). Another is PharmHGT that leverages a unique pharmacophoric-constrained heterogeneous molecule graph and two various transformers to extract chemical properties and predict molecular attributes (Jiang et al., 2023).

We also investigate the problem at other tasks and datasets. Specifically, for the task of IC50 prediction we also perform experiments at the dataset of target BACE1 with a total of 4,636 samples, and we further extend the experiments to the task of Ki prediction for target Carbonic anhydrase I and Carbonic anhydrase II, with 5,307 and 5,487 samples respectively. For all of these datasets we apply the same preprocessing as that of target EGFR, except that taking the negative logarithm form is not applicable to Ki datasets. The results are collectively presented in Table 2, here we choose PharmHGT and SAM-DTA as the example methods for detailed showcase, while The comprehensive collection of results can be found in the appendix.

In summary, extensive experiments demonstrate the generality of the imbalanced distribution of samples by randomized split and the consequent overwhelming of low-similarity samples. The problem will be analyzed and addressed in the following section.

3 SIMILARITY AWARE EVALUATION

In this section we will elaborate the proposed Similarity Aware Evaluation (SAE) which aims at testset with desired distribution. We will exemplify the method for testset that is uniform at similarity-based bins (see Figure 1 for 3 similarity-based bins), and then extend it to other desired distributions.

The split for testset that is uniform at similarity-based bins can be formulated as a combination optimization problem as follows. Given a dataset $X = \{x_i, i = 1, 2, ..., N\}$, a pairwise similarity matrix $\{s_{ij} \in [0, 1], s_{ii} = 0, i = 1, 2, ..., N; j = 1, 2, ..., N\}$, a ratio α, and K bins with boundaries $\{b_k, k = 0, 1, 2, ..., K\}$, find a subset (testset) $X_{ts} \subset X, |X_{ts}| = \alpha N$, such that

$$f(X_{ts}) = \sum_{k=1}^{K} \frac{(o_k - \alpha N/K)^2}{\alpha N/K} \tag{3}$$

is minimized, where

$$o_k = |\{x_i \in X_{ts} : b_{k-1} < r_i \leq b_k\}| \tag{4}$$

$$r_i = \max_{x_j \in X_{tr}} s_{ij} \tag{5}$$

$$X_{tr} = X - X_{ts} \tag{6}$$

X_{tr} denotes the trainset, r_i the similarity of x_i to the trainset, and o_k the count for each of the K bins. Note that the objective function f is essentially the χ^2 statistics in the Chi-Square (χ^2) Test, where o_k is the observed count in each bin and $\alpha N/K$ the expected. Note also that we specially set $s_{ii} = 0$ in the pairwise similarity matrix. This has no effect to the problem itself, but can avoid that r_i falls trivially to 1 due to the maximum operation for the relaxed problem below.

The combination optimization problem is infeasible to solve for optimum. As a result, we relax it to a continuous optimization problem where samples are allowed to coexist in trainset and testset by introduction of the weights $\{w_i \in [0, 1], i = 1, 2, ..., N\}$ and by $|X_{ts}| = \alpha N$ we have constraints $\sum_i w_i = \alpha N$. Next, we have to deal with non-differentiable operations in the objective function f including taking the maximum and counting in similarity-based bins. For the maximum function in calculation of r_i, we approximate it by the LogSumExp operation with a hyper-parameter β,

$$r_i = \max_{x_j \in X_{tr}} s_{ij} = \max_j (1 - w_j) s_{ij} \approx \frac{1}{\beta} \log \sum_j \exp\left(\beta(1 - w_j) s_{ij}\right) \tag{7}$$

In terms of counting for similarity-based bins in calculation of o_k, we approximate the discrete event of a sample falling into a specific bin by a continuous score which depends on how far r_i of the sample deviates from the center of the bin. The score function is defined following the bell-shaped normal distribution with the center of the bin as the expectation and a tunable standard deviation. For a sample, scores across all bins are the normalized. Specifically, denote $c_k = (b_{k-1} + b_k)/2$ as

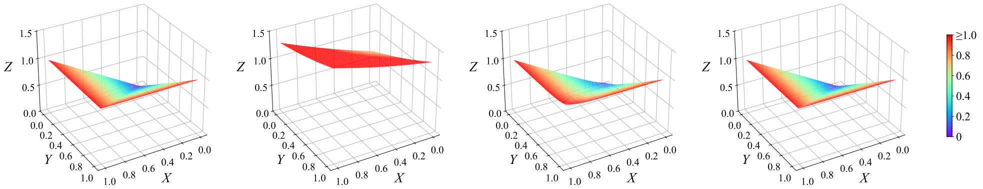

(a) Max (b) $\beta = 1$ (c) $\beta = 10$ (d) $\beta = 100$

Figure 2: Impact of the hyper-parameter β on the approximation of the maximum function in Eq. 7. To illustrate this impact, we consider a simplified scenario involving only two random variables: X and Y. (a) $Z = Max(X, Y)$; (b-d) $Z = 1/\beta \log(\exp(\beta X) + \exp(\beta Y))$. A larger value of β results in a more accurate approximation, with $\beta = 100$ yielding an excellent result.

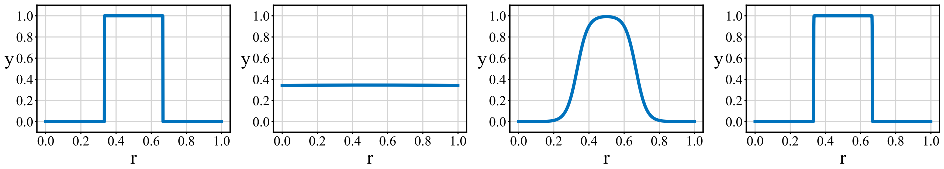

(a) $\mathbb{I}(\frac{1}{3} < r \leq \frac{2}{3})$ (b) $\sigma = 1$ (c) $\sigma = 0.1$ (d) $\sigma = 0.01$

Figure 3: Influence of the hyper-parameter σ in Eq. 12. we analyze a specific case where $K = 3, b_k = k/3, c_k = (2k-1)/6$. (a) $y = \mathbb{I}(b_1 < r \leq b_2)$; (b-d) $y = \exp\left((-(r-c_2)^2/(2\sigma^2)\right) / \sum_{k=1}^{3} \exp\left(-(r-c_k)^2/(2\sigma^2)\right)$. A decrease in the value of σ leads to a more precise estimation, with $\sigma = 0.01$ producing an outstanding result.

the center of each bin, σ_k as the tunable standard deviation, we have:

$$\begin{aligned} o_k &= |\{x_i \in X_{ts} : b_{k-1} < r_i \leq b_k\}| && (8) \\ &= \sum_i w_i \mathbb{I}(b_{k-1} < r_i \leq b_k) && (9) \\ &\approx \sum_i w_i \frac{\frac{1}{\sqrt{2\pi}\sigma_k} \exp\left(-(r_i - c_k)^2/(2\sigma_k^2)\right)}{\sum_{k'} \frac{1}{\sqrt{2\pi}\sigma_{k'}} \exp\left(-(r_i - c_{k'})^2/(2\sigma_{k'}^2)\right)} && (10) \\ & && (11) \end{aligned}$$

where $\mathbb{I}$ is the indicator function. In this paper, we set $\sigma_k = \sigma, k = 1, 2, ..., K$. Thus, we obtain the following expression:

$$o_k \approx \sum_i w_i \frac{\exp\left(-(r_i - c_k)^2/(2\sigma^2)\right)}{\sum_{k'} \exp\left(-(r_i - c_{k'})^2/(2\sigma^2)\right)} = \sum_i w_i \underset{k}{softmax}\left(-\frac{(r_i - c_k)^2}{2\sigma^2}\right) \quad (12)$$

Figure 2 and Figure 3 illustrates the error induced by these two differentiable approximation, with respect to hyper-parameter β and σ, respectively. In Figure 2 we compare β between values of 1, 10 and 100 and plot the surface for a special case of maximum over two variables. It can be seen that a larger β achieves a better approximation, but is also prone to overflow in practice. We use $\beta = 100$ throughout the paper. For Figure 3, on the other hand, we show the comparison of σ values between 1, 0.1 and 0.01 for an example case of the indicator of the second bin for a 3-bin setting $b_k = k/3$. The degree of approximation gets better when value of σ decreases, and is pretty well when $\sigma = 0.01$. For the sake of flexibility, we set $\sigma_k = 0.1(b_k - b_{k-1})$ in rest of the paper.

At the moment we seem to be ready to arrive at the approximated optimization function. However, in practice we find that the approximation error induced by relaxing w_i from $\{0, 1\}$ to $[0, 1]$ is not negligible. In fact, a considerable proportion of w_i solved is neither near 0 nor 1. To address this issue, we are inspired from the concept of entropy, and propose to add a regularization term,

$$l_{reg} = -\lambda \sum_i (w_i \log(w_i) + (1 - w_i) \log(1 - w_i)) \quad (13)$$

where λ is a hyper-parameter that balances between objective function and the regularization term. Finally, we have the optimization problem,

$$\underset{w_i}{minimize} \quad \sum_{k=1}^{K} \frac{(o_k - \alpha N/K)^2}{\alpha N/K} + l_{reg} \tag{14}$$

$$subject\ to \quad \sum_{i} w_i = \alpha N \tag{15}$$

$$0 \leq w_i \leq 1, i = 1, 2, ..., N \tag{16}$$

where

$$o_k = \sum_i w_i \underset{k}{softmax} \left(-\frac{(r_i - c_k)^2}{2\sigma^2} \right) \tag{17}$$

$$r_i = \frac{1}{\beta} \log \sum_j \exp\left(\beta(1 - w_j)s_{ij}\right) \tag{18}$$

$$l_{reg} = -\lambda \sum_i \left(w_i \log(w_i) + (1 - w_i)\log(1 - w_i)\right) \tag{19}$$

Note that the optimization problem has no closed-form solution, and hence we have resorted to Lagrangian multipliers with numerical method implemented by PyTorch and Cooper.

For other desired distributions, one can modify the objective function f in a straightforward way while the approximation tricks and regularization term can be retained, and the resulting optimization function can also be solved by Lagrangian multipliers with numerical method. Generally, if the expected count in each bin is $e_k, k = 1, 2, ..., K$, the objective function can be readily modified as

$$\sum_{k=1}^{K} \frac{(o_k - e_k)^2}{e_k} + l_{reg} \tag{20}$$

4 EXPERIMENTS

4.1 BALANCED SPLIT

In Section 2, we demonstrated that within the context of the randomized split, suboptimal performance on low-similarity samples does not significantly impact the overall performance, as they only occupy a negligible proportion. To avoid disregarding samples with low similarity, we implemented a “balanced split” using similarity aware split strategy to achieve a uniformly distributed testset across various similarity bins ($[1/3, 2/3]$, $(1/3, 2/3]$, $(2/3, 1]$). Figure 1 shows a comparison of randomized split and SAE (balanced) split at IC50 for EGFR. The randomized split strategy yielded a case that 88% of test samples have high similarity ($> 2/3$) to the trainset, while our split strategy guarantees a more evenly distributed range of similarities. The evaluation at the SAE (balanced) split reveals that the performance of each model aligns with the respective similarity levels. Hence, our SAE (balanced) split provides a more accurate representation of the performance of each method.

Additional results at other tasks and datasets are delineated in Table 2. Given the space constraint, we provide experimental results of two representative DTA prediction methods. Notably, analogous phenomena are observed across the remaining three datasets. The comprehensive collection of results can be found in the appendix.

4.2 MIMIC SPLIT

In scenarios when prior knowledge about the external dataset, such as the distribution of similarity to existing samples, is available for the deployment of the DTA prediction method, we can construct an internal testset that closely mirrors this distribution. This strategy enables us to select optimal hyper-parameter configurations for the deployment of the DTA prediction method, thereby enhancing its performance on the external dataset.

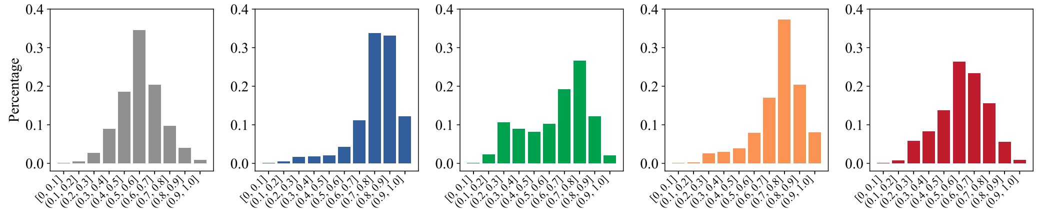

(a) External Testset (b) Random (c) Scaffold (d) SIMPD (e) SAE (mimic)

Figure 4: The similarity distribution of the internal testset across different split strategies. (b) Randomized split leads to a scenario where most internal test samples are highly similar to the trainset. (c) Scaffold split produces a more balanced distribution. (d) SIMPD split yields a distribution similar to the random split. (e) Our SAE (mimic) split brings the internal testset's distribution closest to that of the external testset.

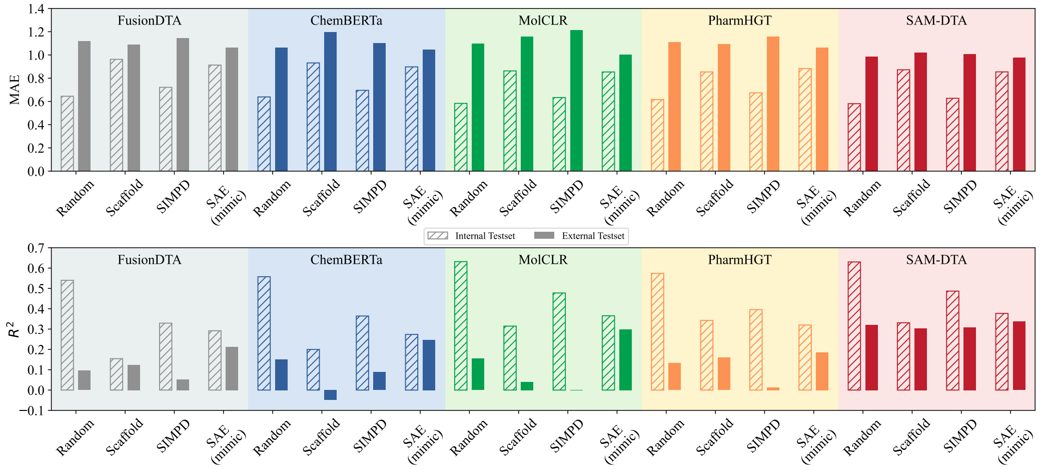

Figure 5: Comparison on the generalization ability of different split strategies at IC50 for EGFR across five DTA prediction methods. The external testset performance of the mimic split surpasses that of other split strategies.

We conducted experiments on the task of predicting IC50 values using the EGFR target dataset. Specifically, 70.2% samples were procured from ChEMBL (Zdrazil et al., 2024), while the remaining samples were obtained from PubChem (Kim et al., 2023), the US Patent and the scientific literature available in BindingDB (Gilson et al., 2016). For our analysis, we classified the ChEMBL-derived samples as internal data, while those obtained from the other sources as external testset. We first computed the similarity distribution between the external testset and the internal data, as shown in Figure 4 (a). Subsequently, we employed the Randomized split, Scaffold split, and SIMPD split (Landrum et al., 2023) to split the internal data into a trainset and an internal testset with a ratio of 70% and 30%. The similarity distributions between the internal testset and the trainset for these splits are depicted in Figure 4 (b-d), respectively. Finally, we utilized the proposed split strategy to split the internal data, thereby mimicking the similarity distribution observed in the external testset. The results are illustrated in Figure 4 (e). We refer to this split strategy as “mimic split”.

For the DTA prediction methods, we searched for hyper-parameters such as optimizer, learning rate, batch size and other relevant hyper-parameters. Details of the hyper-parameters for each method are provided in the appendix. Experimental results are shown in Figure 5, our SAE (mimic) split strategy consistently yields optimal hyper-parameter sets for all the five DTA prediction methods. Among the various split strategies, the scores of our SAE (mimic) split on the internal testset are the most closely aligned with those on the external testset.

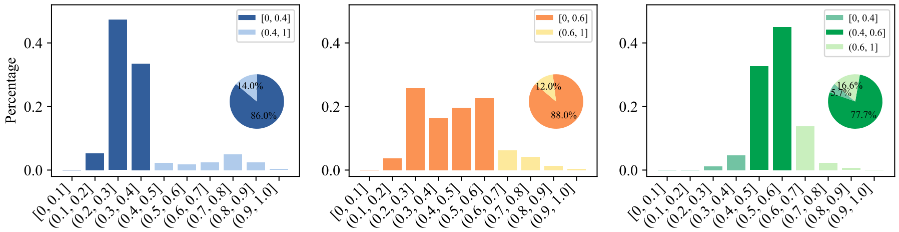

(a) Test data distribution with 0~0.4 split

(b) Test data distribution with 0~0.6 split

(c) Test data distribution with 0.4~0.6 split

Figure 6: Other applications of our split strategy on the IC50 dataset of target EGFR. (a) 86% of the test samples satisfied the desired distribution with a maximum similarity of 0.4, (b) 88% of the test samples met the criteria for a maximum similarity of 0.6, and (c) 77.7% of the test samples fulfilled the requirements for a similarity range between 0.4 and 0.6.

4.3 OTHER APPLICATIONS

Beyond achieving balanced splits, our strategy supports distributions with maximum similarities of 0.4 or 0.6, or a range between 0.4 and 0.6. In a 7:3 train-test split on the EGFR target's IC50 dataset (Figure 6), SAE ensured 86%, 88%, and 77.7% of test samples met the criteria, respectively. This underscores the flexibility of the strategy in accommodating diverse split needs. Moreover, since SAE can flexibly achieve desired distributions by capturing the similarity between pairs of data samples, it can also be applied to QSAR scenarios, including ADMET prediction, drug design (De et al., 2022; Tropsha et al., 2024), as well as the prediction of protein-protein interactions (PPI) (Sharma & Bhatia, 2021) and drug-drug interactions (DDI) (Dmitriev et al., 2019).

5 RELATED WORKS

When evaluating machine learning methods, it is essential to set aside a testset for benchmarking (Wu et al., 2018). The similarity between the trainset and the testset significantly influences the performance of these methods (Sheridan et al., 2004; Cherkasov et al., 2014; Pahikkala et al., 2015; Sieg et al., 2019; Nguyen et al., 2022; Atas Guvenilir & Doğan, 2023; Harren et al., 2024). However, in the field of chemical data, imbalanced data distributions are an inherent and unavoidable challenge (Harren et al., 2024; Yang et al., 2020; Tossou et al., 2024). Therefore, it is crucial to design dataset split strategies that account for these imbalances and ensure meaningful evaluation of model performance (Li & Yang, 2017; Sheridan et al., 2022). The commonly used random splitting method may fail to meet the requirements due to inherent data bias. A typical solution is to exclude all samples in the trainset that are similar to those in the test set (Li et al., 2021; Scantlebury et al., 2023; Luo et al., 2024; 2017; Wan et al., 2019; Atas Guvenilir & Doğan, 2023). Recently, several advanced split strategies have been proposed, including scaffold split (Bemis & Murcko, 1996; Fang et al., 2022; Zhou et al., 2023; Liu et al., 2024), time split (Guan et al., 2023; Stärk et al., 2022), stratified split (Wu et al., 2018; Chen et al., 2022), physicochemical properties-based split (Kalemati et al., 2024), cold-drug split (Huang et al., 2021), and SIMPD (Landrum et al., 2023), among others.

6 CONCLUSION

In this paper, we show the generality of the imbalanced distribution of samples by randomized split and the consequent overwhelming of low-similarity samples. To address the issue, we proposed a novel and flexible similarity aware split strategy for testset to achieve a desired distribution like uniform discrete distribution, which can deliver a comprehensive evaluation for various drug-target binding affinity prediction algorithms. Furthermore, we utilized the similarity aware split to create a "mimic split", splitting the trainset and internal testset by replicating the distribution found in an external testset. Our mimic split consistently aids in selecting the optimal hyper-parameter across various deep learning methods. In the end, our split strategy allows for the generation of distributions with minimum or maximum similarity constraints as needed.

REFERENCES

Heba Askr, Enas Elgeldawi, Heba Aboul Ella, Yaseen AMM Elshaier, Mamdouh M Gomaa, and Aboul Ella Hassanien. Deep learning in drug discovery: an integrative review and future challenges. *Artificial Intelligence Review*, 56(7):5975–6037, 2023.

Heval Atas Guvenilir and Tunca Doğan. How to approach machine learning-based prediction of drug/compound–target interactions. *Journal of Cheminformatics*, 15(1):16, 2023.

Dávid Bajusz, Anita Rácz, and Károly Héberger. Why is tanimoto index an appropriate choice for fingerprint-based similarity calculations? *Journal of cheminformatics*, 7:1–13, 2015.

Guy W Bemis and Mark A Murcko. The properties of known drugs. 1. molecular frameworks. *Journal of medicinal chemistry*, 39(15):2887–2893, 1996.

Ayan Chatterjee, Robin Walters, Zohair Shafi, Omair Shafi Ahmed, Michael Sebek, Deisy Gysi, Rose Yu, Tina Eliassi-Rad, Albert-László Barabási, and Giulia Menichetti. Improving the generalizability of protein-ligand binding predictions with ai-bind. *Nature communications*, 14(1): 1989, 2023.

Hongming Chen, Ola Engkvist, Yinhai Wang, Marcus Olivecrona, and Thomas Blaschke. The rise of deep learning in drug discovery. *Drug discovery today*, 23(6):1241–1250, 2018.

Wenlin Chen, Austin Tripp, and José Miguel Hernández-Lobato. Meta-learning adaptive deep kernel gaussian processes for molecular property prediction. *arXiv preprint arXiv:2205.02708*, 2022.

Artem Cherkasov, Eugene N Muratov, Denis Fourches, Alexandre Varnek, Igor I Baskin, Mark Cronin, John Dearden, Paola Gramatica, Yvonne C Martin, Roberto Todeschini, et al. Qsar modeling: where have you been? where are you going to? *Journal of medicinal chemistry*, 57 (12):4977–5010, 2014.

Seyone Chithrananda, Gabriel Grand, and Bharath Ramsundar. Chemberta: large-scale self-supervised pretraining for molecular property prediction. *arXiv preprint arXiv:2010.09885*, 2020.

Kangway V Chuang, Laura M Gunsalus, and Michael J Keiser. Learning molecular representations for medicinal chemistry: miniperspective. *Journal of Medicinal Chemistry*, 63(16):8705–8722, 2020.

Priyanka De, Supratik Kar, Pravin Ambure, and Kunal Roy. Prediction reliability of qsar models: an overview of various validation tools. *Archives of Toxicology*, 96(5):1279–1295, 2022.

Tim Dettmers, Artidoro Pagnoni, Ari Holtzman, and Luke Zettlemoyer. Qlora: Efficient finetuning of quantized llms. *Advances in Neural Information Processing Systems*, 36, 2024.

Alexander V Dmitriev, Alexey A Lagunin, Dmitry A Karasev, Anastasia V Rudik, Pavel V Pogodin, Dmitry A Filimonov, and Vladimir V Poroikov. Prediction of drug-drug interactions related to inhibition or induction of drug-metabolizing enzymes. *Current Topics in Medicinal Chemistry*, 19(5):319–336, 2019.

Xiaomin Fang, Lihang Liu, Jieqiong Lei, Donglong He, Shanzhuo Zhang, Jingbo Zhou, Fan Wang, Hua Wu, and Haifeng Wang. Geometry-enhanced molecular representation learning for property prediction. *Nature Machine Intelligence*, 4(2):127–134, 2022.

Jose Gallego-Posada and Juan Ramirez. Cooper: a toolkit for Lagrangian-based constrained optimization. `https://github.com/cooper-org/cooper`, 2022.

Michael K Gilson, Tiqing Liu, Michael Baitaluk, George Nicola, Linda Hwang, and Jenny Chong. Bindingdb in 2015: a public database for medicinal chemistry, computational chemistry and systems pharmacology. *Nucleic acids research*, 44(D1):D1045–D1053, 2016.

Jiaqi Guan, Wesley Wei Qian, Xingang Peng, Yufeng Su, Jian Peng, and Jianzhu Ma. 3d equivariant diffusion for target-aware molecule generation and affinity prediction. *arXiv preprint arXiv:2303.03543*, 2023.

Tobias Harren, Torben Gutermuth, Christoph Grebner, Gerhard Hessler, and Matthias Rarey. Modern machine-learning for binding affinity estimation of protein–ligand complexes: Progress, opportunities, and challenges. *Wiley Interdisciplinary Reviews: Computational Molecular Science*, 14(3):e1716, 2024.

Zhiqiang Hu, Wenfeng Liu, Chenbin Zhang, Jiawen Huang, Shaoting Zhang, Huiqun Yu, Yi Xiong, Hao Liu, Song Ke, and Liang Hong. Sam-dta: a sequence-agnostic model for drug–target binding affinity prediction. *Briefings in Bioinformatics*, 24(1):bbac533, 2023.

Kexin Huang, Tianfan Fu, Wenhao Gao, Yue Zhao, Yusuf Roohani, Jure Leskovec, Connor W Coley, Cao Xiao, Jimeng Sun, and Marinka Zitnik. Therapeutics data commons: Machine learning datasets and tasks for drug discovery and development. *arXiv preprint arXiv:2102.09548*, 2021.

James P Hughes, Stephen Rees, S Barrett Kalindjian, and Karen L Philpott. Principles of early drug discovery. *British journal of pharmacology*, 162(6):1239–1249, 2011.

Yinghui Jiang, Shuting Jin, Xurui Jin, Xianglu Xiao, Wenfan Wu, Xiangrong Liu, Qiang Zhang, Xiangxiang Zeng, Guang Yang, and Zhangming Niu. Pharmacophoric-constrained heterogeneous graph transformer model for molecular property prediction. *Communications Chemistry*, 6(1):60, 2023.

Mahmood Kalemati, Mojtaba Zamani Emani, and Somayyeh Koohi. Dcgan-dta: Predicting drug-target binding affinity with deep convolutional generative adversarial networks. *BMC genomics*, 25(1):411, 2024.

Mostafa Karimi, Di Wu, Zhangyang Wang, and Yang Shen. Deepaffinity: interpretable deep learning of compound–protein affinity through unified recurrent and convolutional neural networks. *Bioinformatics*, 35(18):3329–3338, 2019.

Sunghwan Kim, Jie Chen, Tiejun Cheng, Asta Gindulyte, Jia He, Siqian He, Qingliang Li, Benjamin A Shoemaker, Paul A Thiessen, Bo Yu, et al. Pubchem 2023 update. *Nucleic acids research*, 51(D1):D1373–D1380, 2023.

Sowmya Ramaswamy Krishnan, Navneet Bung, Gopalakrishnan Bulusu, and Arijit Roy. Accelerating de novo drug design against novel proteins using deep learning. *Journal of Chemical Information and Modeling*, 61(2):621–630, 2021.

Damjan Krstajic, Ljubomir J Buturovic, David E Leahy, and Simon Thomas. Cross-validation pitfalls when selecting and assessing regression and classification models. *Journal of cheminformatics*, 6:1–15, 2014.

Gregory A Landrum, Maximilian Beckers, Jessica Lanini, Nadine Schneider, Nikolaus Stiefl, and Sereina Riniker. Simpd: an algorithm for generating simulated time splits for validating machine learning approaches. *Journal of cheminformatics*, 15(1):119, 2023.

J Thomas Leonard and Kunal Roy. On selection of training and test sets for the development of predictive qsar models. *QSAR & Combinatorial Science*, 25(3):235–251, 2006.

Hongjian Li, Gang Lu, Kam-Heung Sze, Xianwei Su, Wai-Yee Chan, and Kwong-Sak Leung. Machine-learning scoring functions trained on complexes dissimilar to the test set already outperform classical counterparts on a blind benchmark. *Briefings in bioinformatics*, 22(6):bbab225, 2021.

Shiwei Li, Sanan Wu, Lin Wang, Fenglei Li, Hualiang Jiang, and Fang Bai. Recent advances in predicting protein–protein interactions with the aid of artificial intelligence algorithms. *Current Opinion in Structural Biology*, 73:102344, 2022.

Yang Li and Jianyi Yang. Structural and sequence similarity makes a significant impact on machine-learning-based scoring functions for protein–ligand interactions. *Journal of chemical information and modeling*, 57(4):1007–1012, 2017.

Yanjun Li, Mohammad A Rezaei, Chenglong Li, and Xiaolin Li. Deepatom: A framework for protein-ligand binding affinity prediction. In *2019 IEEE International Conference on Bioinformatics and Biomedicine (BIBM)*, pp. 303–310. IEEE, 2019.

Zhiyuan Liu, Yaorui Shi, An Zhang, Enzhi Zhang, Kenji Kawaguchi, Xiang Wang, and Tat-Seng Chua. Rethinking tokenizer and decoder in masked graph modeling for molecules. *Advances in Neural Information Processing Systems*, 36, 2024.

Ding Luo, Dandan Liu, Xiaoyang Qu, Lina Dong, and Binju Wang. Enhancing generalizability in protein–ligand binding affinity prediction with multimodal contrastive learning. *Journal of Chemical Information and Modeling*, 64(6):1892–1906, 2024.

Yunan Luo, Xinbin Zhao, Jingtian Zhou, Jinglin Yang, Yanqing Zhang, Wenhua Kuang, Jian Peng, Ligong Chen, and Jianyang Zeng. A network integration approach for drug-target interaction prediction and computational drug repositioning from heterogeneous information. *Nature communications*, 8(1):573, 2017.

Neann Mathai, Ya Chen, and Johannes Kirchmair. Validation strategies for target prediction methods. *Briefings in bioinformatics*, 21(3):791–802, 2020.

Nelson RC Monteiro, Carlos JV Simões, Henrique V Ávila, Maryam Abbasi, José L Oliveira, and Joel P Arrais. Explainable deep drug–target representations for binding affinity prediction. *BMC bioinformatics*, 23(1):237, 2022.

Thin Nguyen, Hang Le, Thomas P Quinn, Tri Nguyen, Thuc Duy Le, and Svetha Venkatesh. Graphdta: predicting drug–target binding affinity with graph neural networks. *Bioinformatics*, 37(8):1140–1147, 2021.

Tri Minh Nguyen, Thin Nguyen, and Truyen Tran. Mitigating cold-start problems in drug-target affinity prediction with interaction knowledge transferring. *Briefings in Bioinformatics*, 23(4): bbac269, 2022.

Hakime Öztürk, Arzucan Özgür, and Elif Ozkirimli. Deepdta: deep drug–target binding affinity prediction. *Bioinformatics*, 34(17):i821–i829, 2018.

Tapio Pahikkala, Antti Airola, Sami Pietilä, Sushil Shakyawar, Agnieszka Szwajda, Jing Tang, and Tero Aittokallio. Toward more realistic drug–target interaction predictions. *Briefings in bioinformatics*, 16(2):325–337, 2015.

Yungki Park and Edward M Marcotte. Flaws in evaluation schemes for pair-input computational predictions. *Nature methods*, 9(12):1134–1136, 2012.

Tomasz Puzyn, Aleksandra Mostrag-Szlichtyng, Agnieszka Gajewicz, Michał Skrzyński, and Andrew P Worth. Investigating the influence of data splitting on the predictive ability of qsar/qspr models. *Structural Chemistry*, 22:795–804, 2011.

Jack Scantlebury, Lucy Vost, Anna Carbery, Thomas E Hadfield, Oliver M Turnbull, Nathan Brown, Vijil Chenthamarakshan, Payel Das, Harold Grosjean, Frank Von Delft, et al. A small step toward generalizability: training a machine learning scoring function for structure-based virtual screening. *Journal of Chemical Information and Modeling*, 63(10):2960–2974, 2023.

Smriti Sharma and Vinayak Bhatia. Recent trends in qsar in modelling of drug-protein and protein-protein interactions. *Combinatorial Chemistry & High Throughput Screening*, 24(7):1031–1041, 2021.

Robert P Sheridan. Time-split cross-validation as a method for estimating the goodness of prospective prediction. *Journal of chemical information and modeling*, 53(4):783–790, 2013.

Robert P Sheridan, Bradley P Feuston, Vladimir N Maiorov, and Simon K Kearsley. Similarity to molecules in the training set is a good discriminator for prediction accuracy in qsar. *Journal of chemical information and computer sciences*, 44(6):1912–1928, 2004.

Robert P Sheridan, J Chris Culberson, Elizabeth Joshi, Matthew Tudor, and Prabha Karnachi. Prediction accuracy of production admet models as a function of version: activity cliffs rule. *Journal of Chemical Information and Modeling*, 62(14):3275–3280, 2022.

Jochen Sieg, Florian Flachsenberg, and Matthias Rarey. In need of bias control: evaluating chemical data for machine learning in structure-based virtual screening. *Journal of chemical information and modeling*, 59(3):947–961, 2019.

Jaak Simm, Lina Humbeck, Adam Zalewski, Noe Sturm, Wouter Heyndrickx, Yves Moreau, Bernd Beck, and Ansgar Schuffenhauer. Splitting chemical structure data sets for federated privacy-preserving machine learning. *Journal of cheminformatics*, 13:1–14, 2021.

Yuanbing Song, Jinghua Chen, Wenju Wang, Gang Chen, and Zhichong Ma. Double-head transformer neural network for molecular property prediction. *Journal of Cheminformatics*, 15(1):27, 2023.

Megan Stanley, John F Bronskill, Krzysztof Maziarz, Hubert Misztela, Jessica Lanini, Marwin Segler, Nadine Schneider, and Marc Brockschmidt. Fs-mol: A few-shot learning dataset of molecules. In *Thirty-fifth Conference on Neural Information Processing Systems Datasets and Benchmarks Track (Round 2)*, 2021.

Hannes Stärk, Octavian Ganea, Lagnajit Pattanaik, Regina Barzilay, and Tommi Jaakkola. Equibind: Geometric deep learning for drug binding structure prediction. In *International conference on machine learning*, pp. 20503–20521. PMLR, 2022.

Chunyan Tang, Cheng Zhong, Mian Wang, and Fengfeng Zhou. Fmgnn: A method to predict compound-protein interaction with pharmacophore features and physicochemical properties of amino acids. *IEEE/ACM Transactions on Computational Biology and Bioinformatics*, 20(2): 1030–1040, 2022.

Prudencio Tossou, Cas Wognum, Michael Craig, Hadrien Mary, and Emmanuel Noutahi. Real-world molecular out-of-distribution: Specification and investigation. *Journal of Chemical Information and Modeling*, 64(3):697–711, 2024.

Giovanni A Tricarico, Johan Hofmans, Eelke B Lenselink, Miriam López-Ramos, Marie-Pierre Dréanic, and Pieter FW Stouten. Construction of balanced, chemically dissimilar training, validation and test sets for machine learning on molecular datasets. 2024.

Alexander Tropsha, Olexandr Isayev, Alexandre Varnek, Gisbert Schneider, and Artem Cherkasov. Integrating qsar modelling and deep learning in drug discovery: the emergence of deep qsar. *Nature Reviews Drug Discovery*, 23(2):141–155, 2024.

Fangping Wan, Lixiang Hong, An Xiao, Tao Jiang, and Jianyang Zeng. Neodti: neural integration of neighbor information from a heterogeneous network for discovering new drug–target interactions. *Bioinformatics*, 35(1):104–111, 2019.

Yuyang Wang, Jianren Wang, Zhonglin Cao, and Amir Barati Farimani. Molecular contrastive learning of representations via graph neural networks. *Nature Machine Intelligence*, 4(3):279–287, 2022.

Zhenqin Wu, Bharath Ramsundar, Evan N Feinberg, Joseph Gomes, Caleb Geniesse, Aneesh S Pappu, Karl Leswing, and Vijay Pande. Moleculenet: a benchmark for molecular machine learning. *Chemical science*, 9(2):513–530, 2018.

Zheng Xu, Sheng Wang, Feiyun Zhu, and Junzhou Huang. Seq2seq fingerprint: An unsupervised deep molecular embedding for drug discovery. In *Proceedings of the 8th ACM international conference on bioinformatics, computational biology, and health informatics*, pp. 285–294, 2017.

Jincai Yang, Cheng Shen, and Niu Huang. Predicting or pretending: artificial intelligence for protein-ligand interactions lack of sufficiently large and unbiased datasets. *Frontiers in pharmacology*, 11:69, 2020.

Kevin Yang, Kyle Swanson, Wengong Jin, Connor Coley, Philipp Eiden, Hua Gao, Angel Guzman-Perez, Timothy Hopper, Brian Kelley, Miriam Mathea, et al. Analyzing learned molecular representations for property prediction. *Journal of chemical information and modeling*, 59(8):3370–3388, 2019.

Ziduo Yang, Weihe Zhong, Lu Zhao, and Calvin Yu-Chian Chen. Mgraphdta: deep multiscale graph neural network for explainable drug–target binding affinity prediction. *Chemical science*, 13(3): 816–833, 2022.

Cheng Zhi Ying, Chieu Hai Leong, Liew Wen Xing Alvin, and Chua Jing Yang. Improving the workflow of chemical structure elucidation with morgan fingerprints and the tanimoto coefficient. In *IRC-SET 2020: Proceedings of the 6th IRC Conference on Science, Engineering and Technology, July 2020, Singapore*, pp. 13–24. Springer, 2021.

Weining Yuan, Guanxing Chen, and Calvin Yu-Chian Chen. Fusiondta: attention-based feature polymerizer and knowledge distillation for drug-target binding affinity prediction. *Briefings in Bioinformatics*, 23(1):bbab506, 2022.

Barbara Zdrazil, Eloy Felix, Fiona Hunter, Emma J Manners, James Blackshaw, Sybilla Corbett, Marleen de Veij, Harris Ioannidis, David Mendez Lopez, Juan F Mosquera, et al. The chembl database in 2023: a drug discovery platform spanning multiple bioactivity data types and time periods. *Nucleic acids research*, 52(D1):D1180–D1192, 2024.

Xiao-Chen Zhang, Cheng-Kun Wu, Jia-Cai Yi, Xiang-Xiang Zeng, Can-Qun Yang, Ai-Ping Lu, Ting-Jun Hou, and Dong-Sheng Cao. Pushing the boundaries of molecular property prediction for drug discovery with multitask learning bert enhanced by smiles enumeration. *Research*, 2022: 0004, 2022.

Qichang Zhao, Guihua Duan, Mengyun Yang, Zhongjian Cheng, Yaohang Li, and Jianxin Wang. Attentiondta: Drug–target binding affinity prediction by sequence-based deep learning with attention mechanism. *IEEE/ACM transactions on computational biology and bioinformatics*, 20 (2):852–863, 2022.

Gengmo Zhou, Zhifeng Gao, Qiankun Ding, Hang Zheng, Hongteng Xu, Zhewei Wei, Linfeng Zhang, and Guolin Ke. Uni-mol: A universal 3d molecular representation learning framework. 2023.

A APPENDIX

A.1 RELATED WORKS ON DATA SPLITTING

In molecular machine learning, including general QSAR tasks, the challenge of fair predictive evaluation has been a longstanding issue (Cherkasov et al., 2014). While randomized split remains the most commonly used strategy for data splitting, it is not always the optimal choice for evaluating machine learning methods. Consequently, various alternative split strategies have been developed to better evaluating the machine learning methods:

- *Time split* (Sheridan, 2013; Stärk et al., 2022; Guan et al., 2023) is employed for datasets containing temporal information, where the model is trained on historical data and tested on more recent data. It may effectively replicate the real-world scenarios, however, a significant number of datasets are devoid of time-specific information. In some situations, when the time span is too large or the data distribution changes significantly over time, the model may struggle to perform well on the testset.
- *Scaffold split* (Bemis & Murcko, 1996) is a technique that splits the dataset based on the structural framework of each sample. It is often leveraged in situations involving out-of-distribution data to provide a measure of generalization capabilities (Stanley et al., 2021; Fang et al., 2022; Zhou et al., 2023; Liu et al., 2024). Because scaffold split does not enforce stratification during the partitioning process, it may result in class imbalance (Yang et al., 2019).
- *Stratified split* - also called stratified random sampling - is a sampling method designed to ensure that each fold of a dataset maintains the same distribution of classes as the entire dataset. It achieves this by first dividing the data into different output strata based on class labels and then executes a random partition with the guaranteeing that the entire label range is encompassed within each set (Krstajic et al., 2014; Wu et al., 2018; Mathai et al., 2020; Chen et al., 2022).
- *Cold-drug split* (Huang et al., 2021) is a method for dividing datasets in multi-protein prediction tasks, where the dataset is split based on entity types, such as proteins, drugs, or DNAs. The process begins by randomly splitting the dataset into training, validation, and test sets based on one chosen entity type. Subsequently, all data samples associated with a specific entity are assigned to the same set to ensure no overlap across splits, ensuring that there is no overlap of the chosen entity type across the splits.
- *SIMPD split* (Landrum et al., 2023) mimics temporal splits in scenarios where temporal information is not accessible. This approach was developed by observing and analyzing disparities observed between earlier and subsequent samples within the scope of medicinal chemistry projects.

This challenge is closely intertwined with the broader problem of out-of-distribution (OOD) generalization (Tossou et al., 2024), demonstrating its relevance far beyond the confines of individual tasks such as DTA prediction. In fact, machine learning model tends to perform well when the training set shares a similar distribution with the test set (Leonard & Roy, 2006; Puzyn et al., 2011; Cherkasov et al., 2014). However, the previous split stratigies often yield test sets with distributions that closely mimic the training set (as shown in Figure A.2). Such alignment between the training and test set distributions can lead to overly optimistic assessments of a model's generalization ability, as it fails to account for scenarios where the model is applied to data with significantly different characteristics. SAE provides an effective solution to this issue by enabling more precise control over data distributions through its ability to capture the similarities between data samples. This approach ensures greater adaptability to a wider range of scenarios.

A.2 DISCUSSION ABOUT APPLICATION ON QSAR SCENARIOS

Quantitative Structure-Activity Relationship (QSAR) modeling is a widely used in silico approach for predicting the biological or chemical properties of molecules (De et al., 2022). Previous studies on QSAR (Sheridan et al., 2004) have shown that prediction accuracy is highly correlated with the similarity between the molecule being predicted and its closest neighbor in the training set. This observation is similar to patterns found in the DTA prediction task. Therefore, our SAE method can also be extended to QSAR tasks.

For instance, Krishnan et al. (2021) introduced a de novo drug design method that incorporates a pre-trained model alongside transfer learning to generate novel inhibitors targeting the human JAK2 protein. In this approach, transfer learning was utilized to capture the features of the target-related chemical space. If the characteristics of the target-related chemical space—particularly the distribution of the external dataset—are already well understood, our SAE can be applied to replicate this distribution during the splitting of training and test sets, thereby enhancing the overall performance.

Similarly, in the task of protein-protein interaction prediction, improper construction of the data split among training, validation, and test sets can lead to severe data leakage and overly optimistic results (Li et al., 2022). To address this issue, one proposed solution is to divide the test set into three distinct classes (Park & Marcotte, 2012): C1, where test pairs consist of proteins that are both present in the training set; C2, where test pairs involve one protein present in the training set; and C3, where neither protein in the test pair is found in the training set. Notably, the three classes can be viewed as specific cases of our SAE split strategy. Furthermore, the SAE approach can be flexibly applied to constructing testsets with varying levels of difficulty to more effectively evaluate the model's generalization.

A.3 TIME COMPLEXITY AND SPACE COMPLEXITY ANALYSIS

Given the number of iterations M, the number of samples N, and the number of bins K, we analyze the time complexity of a single iteration in Eq. 14, which involves both forward and backward propagation. During forward propagation, computing o_k involves $O(N \cdot K)$ operations, as it requires iterating over N samples and K bins, with softmax and exponential computations. The computation of r_i is more expensive, requiring $O(N^2)$ operations due to the nested summation over N samples. The regularization term l_{reg} involves a simple summation over N, contributing $O(N)$ operations. Combining these, the time complexity of one forward propagation is dominated by the $O(N^2)$ and $O(N \cdot K)$ terms, resulting in $O(N^2 + N \cdot K)$, which simplifies to $O(N^2)$ because $K \ll N$. For backward propagation, the computation of gradients with respect to w_i involves similar operations, which results in the same complexity of $O(N^2)$. Additionally, the process of checking constraints involves $N + 1$ Lagrangian multipliers. The forward and backward propagation for this constraint-checking step each have a complexity of $O(N)$. Combining all of these components, the time complexity of one iteration is $O(N^2)$, and the total time complexity of SAE across all iterations is $O(M \cdot N^2)$. The overall space complexity of SAE is primarily determined by the storage requirements for s_{ij} and the intermediate values needed for computing gradients from r_i to w_j. As a result, the space complexity is $O(N^2)$.

Empirically, for the IC50 dataset of target EGFR which contains $N = 4,361$ samples, the desired distribution is a uniform over bins $[1/3, 2/3], (1/3, 2/3], (2/3, 1]$. We set the number of iterations to $M = 20,000$. On a single 3090 GPU, SAE completes the process in approximately 270 seconds, utilizing 2,410 MiB of GPU memory.

We would also like to emphasize that SAE is used in the model development stage and as a result, when the model is developed, it will no longer affect the efficiency for high-throughput inference. Note also that SAE needs only to be performed once for a fixed dataset, meaning that it can be reused by different models as long as they are developed on the same dataset. As a result, the time it takes may be overwhelmed by the time used by the heavy model development. When scaling to large datasets, it should be noted that almost all operations within one iteration is parallelable, and thus it will benefit significantly from more powerful GPU devices and distributed computation.

A.4 DISCUSSION ON THE APPLICATION OF SAE TO LARGE-SCALE DATASETS

In pharmacompany (private) drug libraries for early drug discovery, there might be 200,000 to 10^6 samples (Hughes et al., 2011). When scaling to these large datasets, a solution based on sparse matrix is applicable. Specifically, Figure A.1 shows that the majority of pairwise similarities are low. Suppose the desired distribution is uniform over bins $[1/3, 2/3], (1/3, 2/3], (2/3, 1]$ just as in the previous section, over 95% entries in the similarity matrix are less than 1/3 and can be safely set to zero without interference of the results. The time and space complexity can be significantly

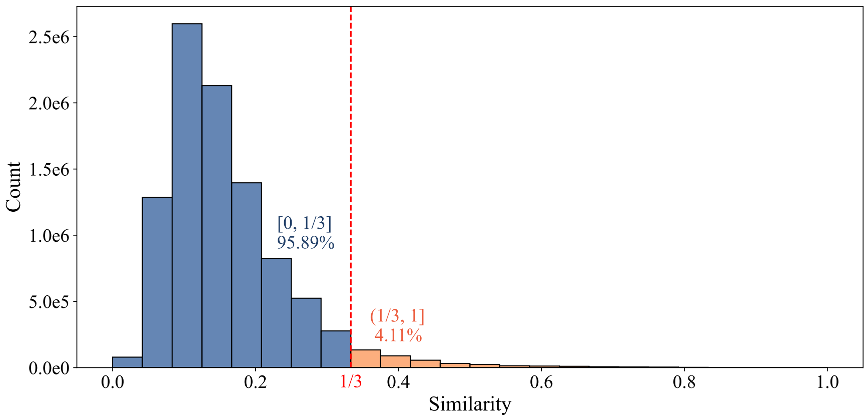

Figure A.1: The similarity distribution of all sample pairs in the IC50 prediction task for the target EGFR. The dataset consists of 4,361 samples, resulting in a total of 9,506,980 pairwise similarity calculations. Among these, 95.89% of the pairs exhibit similarities of no greater than 1/3, while only 4.11% have similarities exceeding 1/3.

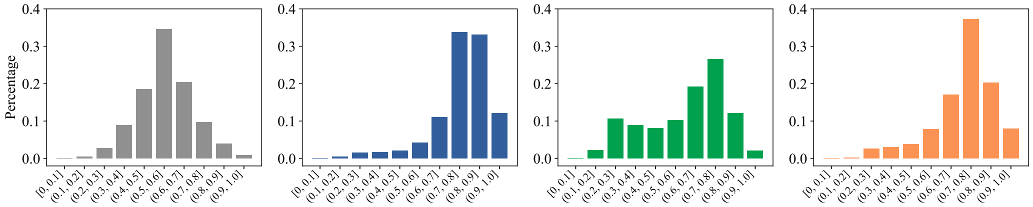

(a) External Testset

(b) Random

(c) Scaffold

(d) SIMPD

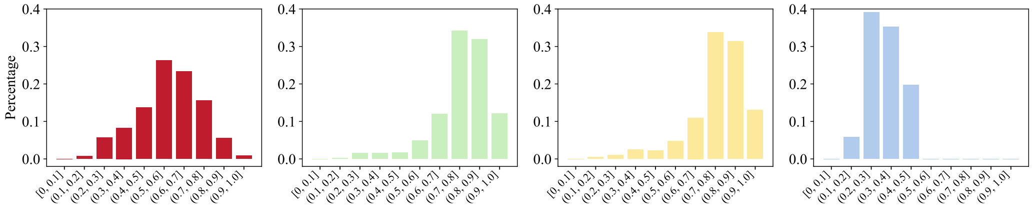

(e) SAE (mimic)

(f) Stratified (max)

(g) Stratified (avg)

(h) Dissimilar

Figure A.2: The similarity distribution of the internal testset across different split strategies. (b) Randomized split leads to a scenario where most internal test samples are highly similar to the trainset. (c) Scaffold split produces a more balanced distribution. (d) SIMPD split yields a distribution similar to the random split. (e) Our SAE (mimic) split brings the internal testset's distribution closest to that of the external testset. (f) Stratified split based on the maximum similarity of each ligand to all others in the dataset. (g) Stratified split based on the average similarity of each ligand to all others in the dataset. (h) Dissimilar split guarantees that the similarity will remain below 0.5.

reduced in this way. Given N = 10^6, the number of pairs with a similarity greater than 1/3 would be approximately $0.05 \cdot N(N-1)/2$, which is about 2.5×10^{10}. We can store these similarities in a sparse format, represented as tuples (Index of sample A, Index of sample B, Similarity value). Each index can be encoded using 20 bits (sufficient to represent 2^{20} = 1,048,576 positions), the similarity value can be quantized into 4 bits (Dettmers et al., 2024). Consequently, the total storage requirement can be calculated as:

$$(20bits + 20bits + 4bits) \times 2.5 \times 10^{10} = 5.5Bytes \times 2.5 \times 10^{10} \approx 128GB$$

This size is manageable and can even be stored in memory.

Table A.1: Comparison on the generalization ability of different split strategies at IC50 for EGFR across five DTA prediction methods.

Split	Method	Internal Test MAE	Internal Test R^2	External Test MAE	External Test R^2
Random	FusionDTA	0.6445	0.5399	1.1198	0.0957
	ChemBERTa	0.6389	0.5574	1.0600	0.1517
	MolCLR	0.5830	0.6318	1.0976	0.1546
	PharmHGT	0.6166	0.5739	1.1107	0.1323
	SAM-DTA	0.5805	0.6301	0.9863	0.3206
Scaffold	FusionDTA	0.9626	0.1544	1.0863	0.1243
	ChemBERTa	0.9314	0.1997	1.1972	-0.0491
	MolCLR	0.8627	0.3145	1.1585	0.0405
	PharmHGT	0.8537	0.3427	1.0930	0.1594
	SAM-DTA	0.8725	0.3311	1.0187	0.3034
SIMPD	FusionDTA	0.7215	0.3292	1.1417	0.0528
	ChemBERTa	0.6954	0.3642	1.1010	0.0878
	MolCLR	0.6334	0.4775	1.2131	-0.0016
	PharmHGT	0.6742	0.3958	1.1588	0.0133
	SAM-DTA	0.6271	0.4867	1.0058	0.3083
Stratified (max)	FusionDTA	0.6753	0.5346	1.0886	0.1517
	ChemBERTa	0.6752	0.5384	1.1504	0.0223
	MolCLR	0.5968	0.6504	1.0917	0.1207
	PharmHGT	0.6092	0.6302	1.0694	0.1811
	SAM-DTA	0.6019	0.6404	1.0345	0.2722
Stratified (avg)	FusionDTA	0.6490	0.5713	1.0957	0.1206
	ChemBERTa	0.6724	0.5191	1.1258	0.0896
	MolCLR	0.5939	0.6368	1.1556	0.1019
	PharmHGT	0.6103	0.5895	1.0938	0.1667
	SAM-DTA	0.6099	0.6159	0.9946	0.3345
Dissimilar	FusionDTA	0.9425	-0.1256	1.2788	-0.1063
	ChemBERTa	0.8927	-0.0139	1.6402	-0.5971
	MolCLR	0.8462	0.0592	1.3355	-0.1366
	PharmHGT	0.9011	-0.0029	1.6006	-0.5237
	SAM-DTA	0.9239	-0.0845	1.2140	-0.0039
SAE (mimic)	FusionDTA	0.9130	0.2919	1.0605	0.2122
	ChemBERTa	0.8976	0.2736	1.0452	0.2477
	MolCLR	0.8536	0.3653	1.0002	0.2981
	PharmHGT	0.8826	0.3200	1.0609	0.1861
	SAM-DTA	0.8545	0.3770	0.9773	0.3367

A.5 SUPPLEMENTARY EXPERIMENTAL RESULTS OF MIMIC SPLIT

For thorough comparison with other split strategies, we implemented stratified split (Wu et al., 2018; Chen et al., 2022) and dissimilar split (Atas Guvenilir & Doğan, 2023) at IC50 for EGFR. For the stratified split, we first compute the pairwise similarities for the full dataset, resulting in a similarity matrix of size $N \times N$ (where N is the number of samples in the dataset, with the diagonal values set to zero). Next, we calculate the maximum/average similarity for each row, yielding a similarity vector of size N, which represents the maximum/average similarity of each ligand to all others in the dataset. Finally, we divide the dataset into K bins based on the maximal/average similarity and perform random sampling within each bin to create the testset. We refer to the two variations of this stratified split strategy as ”Stratified (max),” which uses the maximum similarity for binning, and ”Stratified (avg)”, which uses the average similarity. The similarity distributions of the stratified split are shown in Figure A.2 (f) and Figure A.2 (g). The distribution result of dissimilar split is

Table A.2: Detailed comparison on the generalization ability of different split strategies at IC50 for EGFR across five DTA prediction methods.

Extrenal Test MAE							
Bin	Count	Split	FusionDTA	ChemBERTa	MolCLR	PharmHGT	SAM-DTA
[0, 1/3]	120	Random	1.2442	1.1167	1.2385	1.3261	1.1343
		Scaffold	1.2293	1.2242	1.1630	1.1840	1.1363
		SIMPD	1.4297	1.3223	1.7376	1.3382	1.1179
		Stratified (max)	1.2311	1.1663	1.2414	1.2179	1.1747
		Stratified (avg)	1.5371	1.4478	1.6005	1.3962	1.3666
		Dissimilar	1.4134	1.2363	1.1912	1.2424	1.4161
		SAE (mimic)	1.0626	1.0315	1.1848	1.1082	1.0435
(1/3, 2/3]	1026	Random	1.1416	1.0874	1.0983	1.0989	0.9879
		Scaffold	1.0729	1.2273	1.2021	1.0891	1.0209
		SIMPD	1.1545	1.1272	1.2134	1.1614	1.0158
		Stratified (max)	1.0756	1.1611	1.0927	1.0677	1.0317
		Stratified (avg)	1.0815	1.1450	1.1384	1.0835	0.9808
		Dissimilar	1.3106	1.6954	1.3676	1.6504	1.2513
		SAE (mimic)	1.0531	1.0594	0.9979	1.0606	0.9743
(2/3, 1]	186	Random	0.9559	0.9060	1.0208	1.0516	0.9015
		Scaffold	1.0604	1.0346	0.9449	1.0543	0.9335
		SIMPD	0.9741	0.9022	1.0066	1.0775	0.9191
		Stratified (max)	1.0718	1.0883	1.0017	0.9933	0.9683
		Stratified (avg)	0.9694	0.9047	1.0415	1.0102	0.8967
		Dissimilar	1.0201	1.6720	1.2858	1.6248	0.8773
		SAE (mimic)	1.1003	0.9762	0.8938	1.0322	0.9511

External Test R^2							
Bin	Count	Split	FusionDTA	ChemBERTa	MolCLR	PharmHGT	SAM-DTA
[0, 1/3]	120	Random	-0.5461	-0.5827	-0.5009	-0.6605	-0.2855
		Scaffold	-0.1335	-0.3903	-0.1887	-0.1096	-0.0121
		SIMPD	-0.8717	-0.7917	-1.3400	-0.6245	-0.1181
		Stratified (max)	-0.4278	-0.4195	-0.7345	-0.3873	-0.3106
		Stratified (avg)	-0.8887	-1.0024	-1.1185	-0.5790	-0.3962
		Dissimilar	-0.4209	-0.0067	0.0122	-0.0173	-0.4122
		SAE (mimic)	-0.0736	-0.1140	-0.3105	-0.2592	-0.0783
(1/3, 2/3]	1026	Random	0.0351	0.1066	0.1433	0.1005	0.2950
		Scaffold	0.0987	-0.1211	-0.0502	0.1355	0.2824
		SIMPD	0.0078	0.0332	-0.0169	-0.0337	0.2780
		Stratified (max)	0.1305	-0.0321	0.1016	0.1530	0.2633
		Stratified (avg)	0.1017	0.0476	0.1156	0.1430	0.3188
		Dissimilar	-0.2307	-0.8279	-0.2834	-0.7374	-0.1244
		SAE (mimic)	0.1791	0.1848	0.2632	0.1237	0.3020
(2/3, 1]	186	Random	0.0869	0.1390	-0.0844	0.0577	0.2594
		Scaffold	-0.0967	-0.0351	0.1475	-0.0412	0.2110
		SIMPD	0.1642	0.2476	0.0842	0.0139	0.2880
		Stratified (max)	0.0272	-0.0595	0.1063	0.1111	0.1550
		Stratified (avg)	0.1114	0.2234	0.0081	0.0860	0.3187
		Dissimilar	0.0288	-1.0679	-0.3223	-0.9576	0.2743
		SAE (mimic)	-0.2135	0.1123	0.1807	0.0350	0.1359

shown in Figure A.2 (h). Comparison on the generalization ability of different split strategies is shown in Table A.1. SAE performs better than stratified sampling and dissimilar split with a clear margin.

We also analyse the performance on the different brackets in the external dataset. As is shown in Table A.2, SAE improves performance in the low- and mid-similarity brackets, but not in the high-similarity one. We believe this is because internal testset by SAE has more samples in the low- and mid-similarity brackets and thus performance in these brackets receives more attention compared with other split strategies.

A.6 COMPARISON ACROSS DIFFERENT SIMILARITY MEASURES AND FINGERPRINTS

As for comparison across different similarity measures and fingerprints, we conducted experiments on similarity measure choices including Tanimoto, Cosine, Sokal and Dice, and fingerprint choices including Morgan (ECFP), RDKFP (RDKit) and Avalon. As shown by Table A.3, split results are less affected by similarity measure choices but more influenced by fingerprint choices. In all setting of similarity measures and fingerprints, SAE outperforms other approaches by achieving a split that is closer to the desired distribution (uniform distribution in this case).

Table A.3: Comparison across different similarity measures and fingerprints, the desired distribution is a uniform distribution across the bins [0, 1/3], (1/3, 2/3], and (2/3, 1]. The numbers in this table are presented in the form [Sample counts in the first bin, Sample counts in the second bin, Sample counts in the third bin].

Similarity Measure	Fingerprint	SAE (balanced)	Random	Scaffold	SIMPD	Stratified (max)	Stratified (avg)
Cosine	Morgan	145, 436, 292	0, 33, 840	6, 159, 708	16, 657, 200	0, 32, 841	0, 27, 846
	RDKFP	18, 426, 429	0, 17, 856	1, 78, 794	1, 124, 748	0, 13, 860	1, 14, 858
	Avalon	9, 429, 435	0, 7, 866	0, 21, 852	0, 16, 857	0, 6, 867	0, 6, 867
Sokal	Morgan	292, 289, 292	33, 398, 442	172, 510, 191	689, 126, 58	34, 423, 416	29, 416, 428
	RDKFP	291, 291, 291	19, 80, 774	85, 236, 552	135, 624, 114	14, 82, 777	15, 74, 784
	Avalon	291, 291, 291	7, 63, 803	26, 275, 572	23, 629, 221	8, 76, 789	6, 73, 794
Dice	Morgan	182, 378, 313	0, 33, 840	9, 163, 701	17, 672, 184	0, 34, 839	2, 27, 844
	RDKFP	60, 463, 350	0, 19, 854	2, 83, 788	1, 134, 738	0, 14, 859	1, 14, 858
	Avalon	32, 416, 425	0, 7, 866	0, 26, 847	0, 23, 850	0, 8, 865	0, 6, 867
Tanimoto	Morgan	290, 299, 284	16, 98, 759	80, 273, 520	228, 547, 98	12, 99, 762	13, 99, 761
	RDKFP	289, 292, 292	8, 34, 831	15, 184, 674	2, 635, 236	1, 39, 833	4, 33, 836
	Avalon	220, 325, 328	0, 28, 845	2, 154, 717	1, 324, 548	0, 30, 843	1, 28, 844

Table A.4: Hyper-parameters used in the mimic split experiment for each method, the following search options are derived from the default parameter settings of each method.

Method	Hyper-parameter	Options
SAM-DTA	Optimizer	[Adam, SGD]
	Learning rate	[1e-3, 1e-4, 1e-5]
	Batch size	[10, 32, 64]
MolCLR	Optimizer	[Adam, SGD]
	Learning rate (prediction head, GNN encoder)	[(1e-3, 5e-3), (1e-4, 5e-4), (1e-5, 5e-5)]
	Dropout ratio	[0.3, 0.5]
	Readout pooling	[Mean, Max, Add]
FusionDTA	Optimizer	[Adam, SGD]
	Learning rate	[1e-2, 1e-3, 1e-4]
	Batch size	[128, 256]
	Loss function	[L1, MSE]
PharmHGT	Optimizer	[Adam, SGD]
	Learning rate	[1e-2, 1e-3, 1e-4]
	Activation function	[Sigmoid, ReLU]
	Loss function	[RMSE, MAE]
ChemBERTa	Optimizer	[AdamW, Adafactor]
	Learning rate	[4e-3, 4e-4, 4e-5, 4e-6]
	Batch size	[4, 8, 16]

Table A.5: Variations of *SimilarityToTrainset* related to feature extraction, similarity measure, aggregation functions, and performance metrics. The methods for detailed showcase are FusionDTA and ChemBERTa.

Randomized Split (MAE)						
Bin	Feature: RDKit fingerprint			Feature: Avalon fingerprint		
	Count (Ratio)	FusionDTA	ChemBERTa	Count (Ratio)	FusionDTA	ChemBERTa
[0, 1/3]	8 (0.0092)	1.4442	1.4679	0 (0.0000)	-	-
(1/3, 2/3]	34 (0.0389)	1.1294	1.1306	28 (0.0321)	1.3299	1.2340
(2/3, 1]	831 (0.9519)	0.6407	0.6546	845 (0.9679)	0.6451	0.6623
overall	873 (1.0000)	0.6671	0.6806	873 (1.0000)	0.6671	0.6806
	SimilarityMeasure: Sokal similarity			SimilarityMeasure: Dice coefficient		
[0, 1/3]	33 (0.0378)	1.2751	1.2711	0 (0.0000)	-	-
(1/3, 2/3]	398 (0.4559)	0.7366	0.7234	33 (0.0378)	1.2751	1.2711
(2/3, 1]	442 (0.5063)	0.5591	0.5980	840 (0.9622)	0.6432	0.6574
overall	873 (1.0000)	0.6671	0.6806	873 (1.0000)	0.6671	0.6806
	Aggregation: Top-3			Aggregation: Top-5		
[0, 1/3]	17 (0.0195)	1.1567	1.3484	24 (0.0275)	1.3682	1.3330
(1/3, 2/3]	171 (0.1959)	0.8839	0.8722	240 (0.2749)	0.7861	0.8094
(2/3, 1]	685 (0.7847)	0.6008	0.6162	609 (0.6976)	0.5926	0.6041
overall	873 (1.0000)	0.6671	0.6806	873 (1.0000)	0.6671	0.6806

Randomized Split (R^2)						
Bin	Feature: RDKit fingerprint			Feature: Avalon fingerprint		
	Count (Ratio)	FusionDTA	ChemBERTa	Count (Ratio)	FusionDTA	ChemBERTa
[0, 1/3]	8 (0.0092)	0.2319	0.2536	0 (0.0000)	-	-
(1/3, 2/3]	34 (0.0389)	0.2253	0.1829	28 (0.0321)	0.2166	0.2573
(2/3, 1]	831 (0.9519)	0.5899	0.5796	845 (0.9679)	0.5845	0.5698
overall	873 (1.0000)	0.5697	0.5585	873 (1.0000)	0.5697	0.5585
	SimilarityMeasure: Sokal similarity			SimilarityMeasure: Dice coefficient		
[0, 1/3]	33 (0.0378)	0.0871	0.0615	0 (0.0000)	-	-
(1/3, 2/3]	398 (0.4559)	0.5068	0.5186	33 (0.0378)	0.0871	0.0615
(2/3, 1]	442 (0.5063)	0.6469	0.6117	840 (0.9622)	0.5898	0.5793
overall	873 (1.0000)	0.5697	0.5585	873 (1.0000)	0.5697	0.5585
	Aggregation: Top-3			Aggregation: Top-5		
[0, 1/3]	17 (0.0195)	-0.0685	-0.3530	24 (0.0275)	-0.0237	-0.0345
(1/3, 2/3]	171 (0.1959)	0.4390	0.4408	240 (0.2749)	0.4881	0.4647
(2/3, 1]	685 (0.7847)	0.5930	0.5837	609 (0.6976)	0.5965	0.5903
overall	873 (1.0000)	0.5697	0.5585	873 (1.0000)	0.5697	0.5585

Table A.6: Variations of $\mathit{SimilarityToTrainset}$ related to feature extraction, similarity measure, aggregation functions, and performance metrics. The method for detailed showcase is MolCLR.

Randomized Split (MAE)				
Bin	Feature: RDKit fingerprint		Feature: Avalon fingerprint	
	Count (Ratio)	MolCLR	Count (Ratio)	MolCLR
[0 , 1/3]	8 (0.0092)	1.4442	0 (0.0000)	-
(1/3, 2/3]	34 (0.0389)	1.1294	28 (0.0321)	1.3299
(2/3, 1]	831 (0.9519)	0.6407	845 (0.9679)	0.6451
overall	873 (1.0000)	0.6671	873 (1.0000)	0.6671
	SimilarityMeasure: Sokal similarity		SimilarityMeasure: Dice coefficient	
[0 , 1/3]	33 (0.0378)	1.2751	0 (0.0000)	-
(1/3, 2/3]	398 (0.4559)	0.7366	33 (0.0378)	1.2751
(2/3, 1]	442 (0.5063)	0.5591	840 (0.9622)	0.6432
overall	873 (1.0000)	0.6671	873 (1.0000)	0.6671
	Aggregation: Top-3		Aggregation: Top-5	
[0 , 1/3]	17 (0.0195)	1.1567	24 (0.0275)	1.3682
(1/3, 2/3]	171 (0.1959)	0.8839	240 (0.2749)	0.7861
(2/3, 1]	685 (0.7847)	0.6008	609 (0.6976)	0.5926
overall	873 (1.0000)	0.6671	873 (1.0000)	0.6671

Randomized Split (R^2)				
Bin	Feature: RDKit fingerprint		Feature: Avalon fingerprint	
	Count (Ratio)	MolCLR	Count (Ratio)	MolCLR
[0 , 1/3]	8 (0.0092)	0.2319	0 (0.0000)	-
(1/3, 2/3]	34 (0.0389)	0.2253	28 (0.0321)	0.2166
(2/3, 1]	831 (0.9519)	0.5899	845 (0.9679)	0.5845
overall	873 (1.0000)	0.5697	873 (1.0000)	0.5697
	SimilarityMeasure: Sokal similarity		SimilarityMeasure: Dice coefficient	
[0 , 1/3]	33 (0.0378)	0.0871	0 (0.0000)	-
(1/3, 2/3]	398 (0.4559)	0.5068	33 (0.0378)	0.0871
(2/3, 1]	442 (0.5063)	0.6469	840 (0.9622)	0.5898
overall	873 (1.0000)	0.5697	873 (1.0000)	0.5697
	Aggregation: Top-3		Aggregation: Top-5	
[0 , 1/3]	17 (0.0195)	-0.0685	24 (0.0275)	-0.0237
(1/3, 2/3]	171 (0.1959)	0.4390	240 (0.2749)	0.4881
(2/3, 1]	685 (0.7847)	0.5930	609 (0.6976)	0.5965
overall	873 (1.0000)	0.5697	873 (1.0000)	0.5697

Table A.7: Comparison of Randomized Split and SAE (balanced) Split at IC50 for BACE1, Ki for Carbonic anhydrase I and Carbonic anhydrase II. The methods for detailed showcase are FusionDTA and ChemBERTa.

IC50 for Target BACE1 (MAE)						
Bin	Randomized Split			SAE (balanced) Split		
	Count (Ratio)	FusionDTA	ChemBERTa	Count (Ratio)	FusionDTA	ChemBERTa
[0, 1/3]	10 (0.0108)	1.3020	1.1440	309 (0.3330)	1.2117	1.2503
(1/3, 2/3]	67 (0.0722)	0.7270	0.6719	311 (0.3351)	0.7444	0.6599
(2/3, 1]	851 (0.9170)	0.5105	0.5267	308 (0.3319)	0.5310	0.5352
overall	928 (1.0000)	0.5347	0.5439	928 (1.0000)	0.8292	0.8151
IC50 for Target BACE1 (R^2)						
[0, 1/3]	10 (0.0108)	0.0422	0.3204	309 (0.3330)	-0.5113	-0.5641
(1/3, 2/3]	67 (0.0722)	0.5980	0.6325	311 (0.3351)	0.4238	0.5787
(2/3, 1]	851 (0.9170)	0.6651	0.6446	308 (0.3319)	0.7076	0.7235
overall	928 (1.0000)	0.6755	0.6673	928 (1.0000)	0.4213	0.4548
Ki for Target Carbonic anhydrase I (MAE)						
Bin	Randomized Split			SAE (balanced) Split		
	Count (Ratio)	FusionDTA	ChemBERTa	Count (Ratio)	FusionDTA	ChemBERTa
[0, 1/3]	7 (0.0079)	0.9363	0.9564	264 (0.2983)	1.0252	0.9245
(1/3, 2/3]	205 (0.2316)	0.7086	0.7085	311 (0.3514)	0.7362	0.7228
(2/3, 1]	673 (0.7605)	0.5203	0.5440	310 (0.3503)	0.6181	0.6060
overall	885 (1.0000)	0.5673	0.5854	885 (1.0000)	0.7810	0.7421
Ki for Target Carbonic anhydrase I (R^2)						
[0, 1/3]	7 (0.0079)	0.0634	0.1421	264 (0.2983)	-0.4131	-0.1076
(1/3, 2/3]	205 (0.2316)	0.3536	0.3761	311 (0.3514)	0.2106	0.2829
(2/3, 1]	673 (0.7605)	0.4500	0.4231	310 (0.3503)	0.3532	0.3299
overall	885 (1.0000)	0.4259	0.4161	885 (1.0000)	0.1253	0.2334
Ki for Target Carbonic anhydrase II (MAE)						
Bin	Randomized Split			SAE (balanced) Split		
	Count (Ratio)	FusionDTA	ChemBERTa	Count (Ratio)	FusionDTA	ChemBERTa
[0, 1/3]	8 (0.0087)	0.8465	0.5778	244 (0.2667)	0.9849	0.9314
(1/3, 2/3]	201 (0.2197)	0.6817	0.7419	342 (0.3738)	0.8265	0.7390
(2/3, 1]	706 (0.7716)	0.5605	0.5997	329 (0.3596)	0.6040	0.6072
overall	915 (1.0000)	0.5896	0.6307	915 (1.0000)	0.7888	0.7429
Ki for Target Carbonic anhydrase II (R^2)						
[0, 1/3]	8 (0.0087)	0.0349	0.3581	244 (0.2667)	0.0488	0.2523
(1/3, 2/3]	201 (0.2197)	0.5603	0.4667	342 (0.3738)	0.3416	0.4686
(2/3, 1]	706 (0.7716)	0.5513	0.5146	329 (0.3596)	0.4499	0.4744
overall	915 (1.0000)	0.5570	0.5087	915 (1.0000)	0.3583	0.4659

Table A.8: Comparison of Randomized Split and SAE (balanced) Split at IC50 for BACE1, Ki for Carbonic anhydrase I and Carbonic anhydrase II. The method for detailed showcase is MolCLR.

IC50 for Target BACE1 (MAE)				
Bin	Randomized Split		SAE (balanced) Split	
	Count (Ratio)	MolCLR	Count (Ratio)	MolCLR
[0 , 1/3]	10 (0.0108)	1.2452	309 (0.3330)	1.4141
(1/3, 2/3]	67 (0.0722)	0.6952	311 (0.3351)	0.6940
(2/3, 1]	851 (0.9170)	0.4878	308 (0.3319)	0.4784
overall	928 (1.0000)	0.5109	928 (1.0000)	0.8622
IC50 for Target BACE1 (R^2)				
[0 , 1/3]	10 (0.0108)	-0.0492	309 (0.3330)	-0.9211
(1/3, 2/3]	67 (0.0722)	0.6184	311 (0.3351)	0.5107
(2/3, 1]	851 (0.9170)	0.6919	308 (0.3319)	0.7746
overall	928 (1.0000)	0.6974	928 (1.0000)	0.3713
Ki for Target Carbonic anhydrase I (MAE)				
Bin	Randomized Split		SAE (balanced) Split	
	Count (Ratio)	MolCLR	Count (Ratio)	MolCLR
[0 , 1/3]	7 (0.0079)	0.8510	264 (0.2983)	1.0059
(1/3, 2/3]	205 (0.2316)	0.6141	311 (0.3514)	0.7549
(2/3, 1]	673 (0.7605)	0.4762	310 (0.3503)	0.5755
overall	885 (1.0000)	0.5111	885 (1.0000)	0.7669
Ki for Target Carbonic anhydrase I (R^2)				
[0 , 1/3]	7 (0.0079)	0.3127	264 (0.2983)	-0.3331
(1/3, 2/3]	205 (0.2316)	0.5338	311 (0.3514)	0.1585
(2/3, 1]	673 (0.7605)	0.5598	310 (0.3503)	0.4342
overall	885 (1.0000)	0.5572	885 (1.0000)	0.1552
Ki for Target Carbonic anhydrase II (MAE)				
Bin	Randomized Split		SAE (balanced) Split	
	Count (Ratio)	MolCLR	Count (Ratio)	MolCLR
[0 , 1/3]	8 (0.0087)	1.0278	244 (0.2667)	0.8873
(1/3, 2/3]	201 (0.2197)	0.6882	342 (0.3738)	0.6907
(2/3, 1]	706 (0.7716)	0.5497	329 (0.3596)	0.6232
overall	915 (1.0000)	0.5843	915 (1.0000)	0.7189
Ki for Target Carbonic anhydrase II (R^2)				
[0 , 1/3]	8 (0.0087)	-0.3461	244 (0.2667)	0.2192
(1/3, 2/3]	201 (0.2197)	0.5635	342 (0.3738)	0.5347
(2/3, 1]	706 (0.7716)	0.5964	329 (0.3596)	0.4409
overall	915 (1.0000)	0.5856	915 (1.0000)	0.4740